http://journal.uir.ac.id/index.php/JGEET

E-ISSN : 2541-5794
P-ISSN : 2503-216X

Journal of Geoscience,
Engineering, Environment, and Technology
Vol 9 No 4 2024

RESEARCH ARTICLE

A Hydrogeochemistry Analysis for Quality Determination of Shallow Karstic Groundwater in Western Tuban, Indonesia

Setia Pambudi[1*], Budi Sulistijo[2], Irwan Iskandar[2], Dwi Fitri Yudiantoro[1], Intan Paramita Haty[1], Adam Raka Ekasara[1], Afrilita[1], Dian Rahma Yoni[1], Septyo Uji Pratomo[1]

[1]*Geological Engineering Department, Universitas Pembangunan Nasional Veteran Yogyakarta, Jl. Padjajaran No. 104, Sleman, Yogyakarta, Indonesia, 55283.*
[2]*Mining Engineering Department, Institut Teknologi Bandung, Jl. Ganesa No.10, Bandung, Indonesia, 40132.*

* Corresponding author : setia.pambudi@upnyk.ac.id
Received: Jan 16, 2024; Accepted: Nov 21, 2024.
DOI: 10.25299/jgeet.2024.9.04.15926

Abstract

Groundwater hydrogeochemistry and water quality assessment have been conducted in western Tuban, Indonesia, which is characterized by its karstic features based on physicochemical parameters (pH, electric conductivity, total dissolved solids, hardness, Ca^{2+}, Mg^{2+}, Fe^{3+}, Mn^{2+}, K^{+}, Na^{+}, Li^{+}, NH_4^{+}, HCO_3^{-}, Cl^{-}, SO_4^{2-}, NO_2^{-}, and NO_3^{-}) from 25 shallow groundwater samples. The Piper diagram implies the groundwater is of HCO_3–Ca+Mg type with some Na+K–SO_4+Cl type meaning that the groundwater in Western Tuban is influenced by the silicate minerals weathering, the dissolution of carbonate lithology, and seawater intrusion. Durov diagram shows that the evolution of groundwater is influenced by ion exchange with clay minerals and by mixing with seawater. The Gibbs diagram indicates that the change in the chemistry and quality of groundwater is caused by a dominance of rock-water interaction in the Western Tuban. The water quality assessment based on the USSL and Wilcox diagrams indicates a high level of salinity and relatively low sodium, meaning that the suggested crops should have good salt tolerance, and the cultivated soil should still be able to handle the relatively low sodium level for irrigation.

Keywords: hydrogeochemistry, groundwater, karst, Tuban, irrigation

1. Introduction

Groundwater hydrogeochemistry is a vital field of study that investigates the chemistry of groundwater and the interactions between water and surrounding geological features (Elango and Kannan, 2007). Groundwater quality is vital to the environment as it is an essential resource for drinking, industry, and irrigation (Adimalla et al., 2018; Foster, 2001). The geological formation of the aquifer, its physical properties, and the interaction between groundwater and the surrounding environment determine the groundwater quality. The hydrogeochemistry study of groundwater helps to understand the natural processes that control water chemistry, identify sources of contamination, and monitor changes in water quality over time (Glynn and Plummer, 2005). Geochemical analyses of groundwater can provide information about the element mobility in the water and the potential for groundwater recharge (Blake et al., 2022). This subject is of significance as it directly impacts the management and preservation of water resources, as well as the advancement of sustainable environmental practices.

The groundwater quality may change over time depending on the natural and anthropological conditions in the area (Fitchen, 1988). The pollution entering the aquifer decreases the quality of existing water, especially for drinking (Nijhawan and Howard, 2022). The chemistry of the groundwater depends on several aspects, such as the rock type of the aquifer, recharge system, transmissibility of groundwater, residence time, and anthropological activity (Stevanović, 2015). Karst area is typically dominated by carbonate rocks, and this influences the geochemistry of the groundwater since the aquifer is mostly limestone. The occurrences of caves and underground water systems are typical of a karstic groundwater system (Ford and Williams, 2010). Aquifer structure and groundwater properties in the karstic area can, however, be altered by natural phenomena such as climate change, vegetation change, and karstic porosity features (dissolution fractures and caves) (Antonellini et al., 2019; Kaufmann and Romanov, 2019; Sarrazin et al., 2018; Sullivan et al., 2019).

Hydrogeology in the karstic area is a complex and highly dynamic system that involves the interaction between water, rock, and biological processes. The unique geological characteristics of karst landscapes, such as sinkholes, caves, and underground rivers, create distinct hydrological and hydrochemical features. Karst-related areas are characterized by fast and unpredictable groundwater flow (Parise et al., 2018), which can lead to rapid recharge and discharge of water resources. The hydrogeochemistry of karst-related areas is an essential topic of study that focuses on understanding the chemical composition of groundwater in these unique environments. By investigating the hydrogeochemical processes in karst areas, authors can gain a better understanding of the natural processes that control water quality, identify sources of contamination, and develop sustainable management strategies for these valuable water resources.

2. Study area

The focused area investigated in this study is mostly in the western part of Tuban Regency, between the latitude 6.795° – 6.955° S and longitude 111.8° – 112° E (Figure 1). This area covers the districts of Merakurak, Kerek, Tambakboyo, Jenu, and a small part of Montong. The morphology of Western Tuban is mainly flat in the northern

part close to the coastline with an elevation close to 0 meter and slopy in the southern area with a maximum elevation of 350 meters. Physiography of the study area is surrounded by anticline systems, such as Dander, Ngimbang, Pegat, Lidah, and Sekarorong anticlines, as a result of Randublatung depression (van Bemmelen, 1949) from tectonic uplift in the late Tertiary. This results in ridges with an east-west orientation. There are many karstic features found in the study area, from cave systems to terra rosa, as a result of rock dissolution in the study area. Based on monthly rainfall data, Tuban Regency experiences higher levels of precipitation during the rainy season exceeding 100 mm, while during the dry season, precipitation levels fall below 100 mm despite the start of the season varies in the last three years (Badan Pusat Statistik Kabupaten Tuban, 2023).

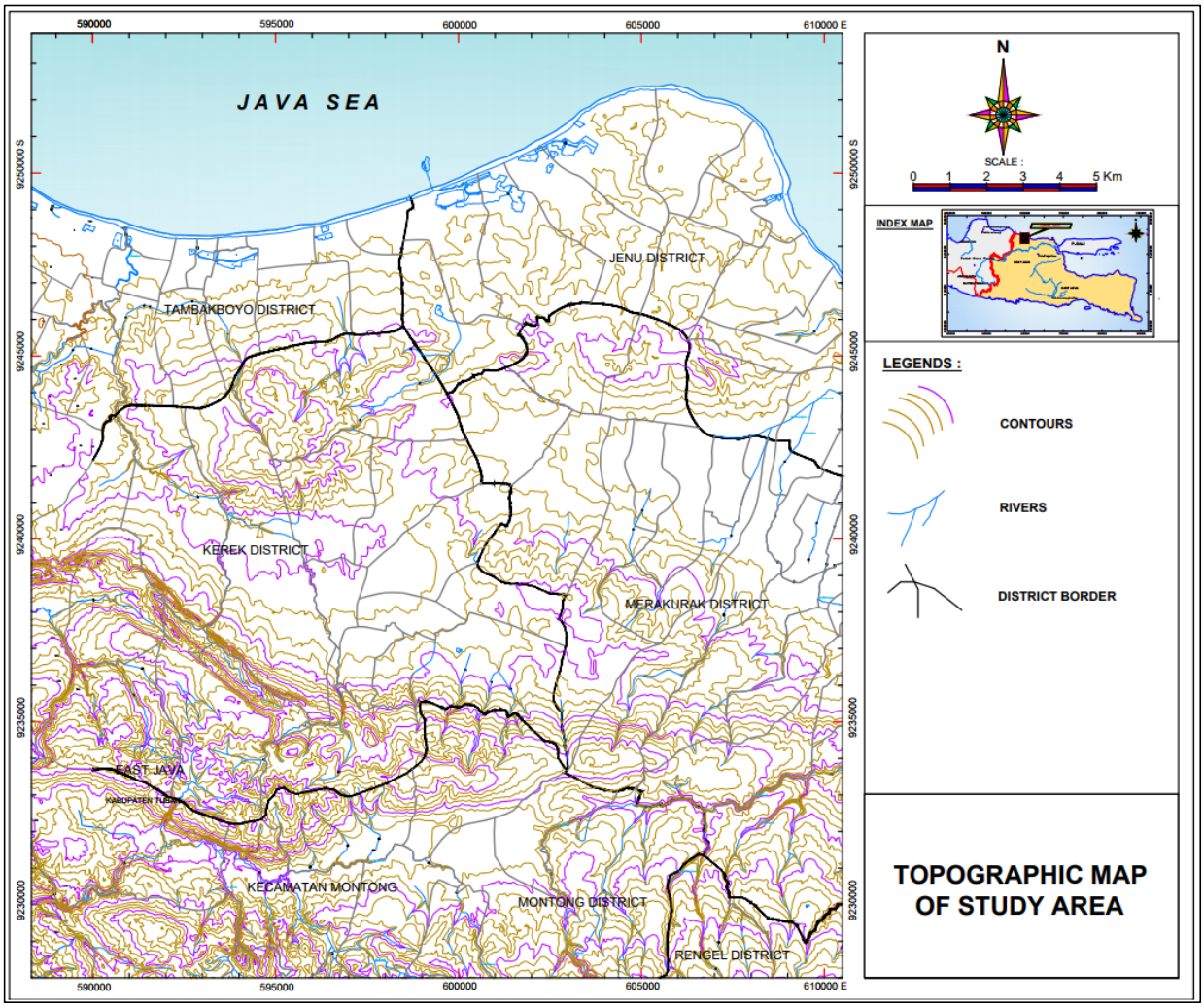

Fig. 1. Topographic map of Western Tuban (BAKOSURTANAL, 1999).

3. Geology

Based on the Jatirogo geological map (Figure 2) by Situmorang et al. (1992), the study area is included in Rembang Line, which comprises carbonate rock unrelated to volcanic activity and formed in the shallow seawater condition close to the paleo-shoreline. The descriptions of the rock found in the Western Tuban are as follows, from the oldest to the most recent:

a. Tawun Member, Tuban Formation (Tmt)

This lithology unit is estimated to have an Early Miocene age. It comprises sandy marl interbedded with bioclastic limestone. Sandy marl has yellowish brown color and is fine to medium grain size. Bioclastic limestone has brownish color, and the grey color comes from foraminifera fossils. This lithology is inexistent as any outcrop in the study area.

b. Ngrayong Member, Tuban Formation (Tmtn)

The Ngrayong Member of the Tuban Formation is dominated by mostly whole claystone though there are some intercalation of clastic limestone and less frequent quartz sandstone (Aditia, 2013). It also contains many foraminifera fossils. Claystone commonly has a yellowish-brown color, and quartz sandstone is commonly found in reddish-brown color with lenses of white quartz sandstone. In some places in this study area, Paciran Formation has contact with the Ngrayong Member, and the contact is defined as an angular unconformity.

c. Bulu Formation (Tmb)

This unit conformably lies over Tuban Formation and has Mid-Eocene age. The unit comprises whitish-grey sandy limestone, sometimes locally clayey and occasionally thin-bedded with sandy marl intercalation.

d. Wonocolo Formation (Tmw)

Wonocolo Formation was deposited over Bulu Formation, and it has Late Miocene age. This formation consists of sandy marl intercalated with sandy limestone and claystone.

e. Ledok Formation (Tml)

This formation conformably lies over Wonocolo Formation and has Late-Miocene to Pliocene. It comprises glauconite sandstone with sandy limestone intercalation.

f. Mundu (Tpm) and Paciran (Tpm) Formations

Over Ledok Formation, there are interfingering Mundu and Paciran Formations with the Pliocene age. Mundu Formation comprises marl, shaly claystone, and marly limestone. On the other hand, Paciran Formation consists of solid reef limestone and dolomite-dominated limestone. This formation dominates the limestone lithology of the study area. The limestone is of wackestone and packstone.

g. Alluvium (Qa)

This unit is the youngest lithology of the study area, aged Holocene. It is sourced from Paciran and Tuban Formation clasts and comprises gravel, sand, shale, and clay

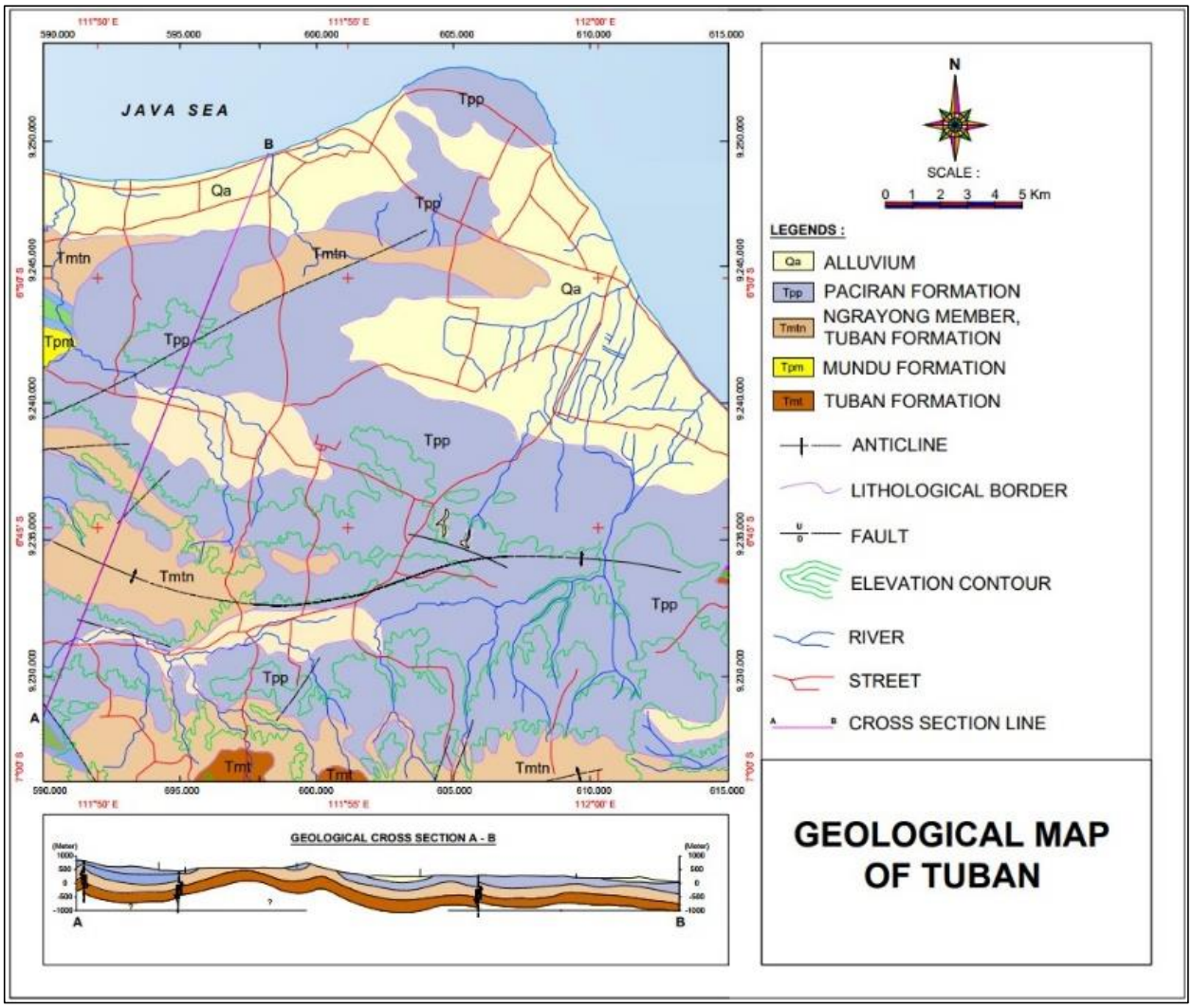

Fig. 2. Geological map of Western Tuban (Asikin, 1992).

4. Methodology

Water samples were collected from various groundwater sources in the western part of Tuban Regency, including eight springs and 17 urban wells. Before sampling, key water properties such as temperature, pH, total dissolved solids (TDS), and electrical conductivity (EC) were measured in situ. Temperature was recorded using a handheld field thermometer, while pH and EC were measured using a calibrated handheld TDS meter to ensure accurate readings.

The water samples were collected in pre-cleaned, opaque bottles to minimize light exposure, and they were carefully stored away from sunlight to prevent any alteration of chemical properties before further analysis. Subsequent geochemical analyses were performed at the Center of Groundwater and Environmental Geology of the Geological Agency (Pusat Airtanah dan Geologi Tata Lingkungan, Badan Geologi).

The chemical analyses measured the concentrations of major cations (Ca^{2+}, Mg^{2+}, Fe^{3+}, Mn^{2+}, K^{+}, Na^{+}, Li^{+}, NH_4^{+}) and anions (HCO_3^{-}, Cl^{-}, SO_4^{2-}, NO_3^{-}). These results were processed and visualized using several methods, including the generation of contour maps through the kriging method, which is suitable for scattered data with potential spatial correlations.

To understand the hydrogeochemical characteristics of the groundwater, the data were plotted on Piper and Durov diagrams, which help identify groundwater types. Additionally, Gibbs diagrams were employed to examine the processes influencing groundwater evolution. The United States Salinity Laboratory (USSL) and Wilcox diagrams were used to evaluate groundwater suitability for agricultural and domestic use, assessing salinity and sodium hazard levels.

5. Results and discussions

5.1 Physical properties of the groundwater

The physical properties, cations, and anions of the groundwater samples are presented in Table 1. In-situ temperatures range from 28.6 to 36.7°C (Figure 3a). Two water samples exhibit elevated temperatures above 34°C. One sample is from a hot spring, likely a geothermal manifestation, though there is no active volcanism in the vicinity. The extinct Mount Lasem, located about 25 km to the west, may influence the geothermal gradient in the region. Another source has an elevated temperature due to prolonged mechanical pumping, which likely caused localized heating.

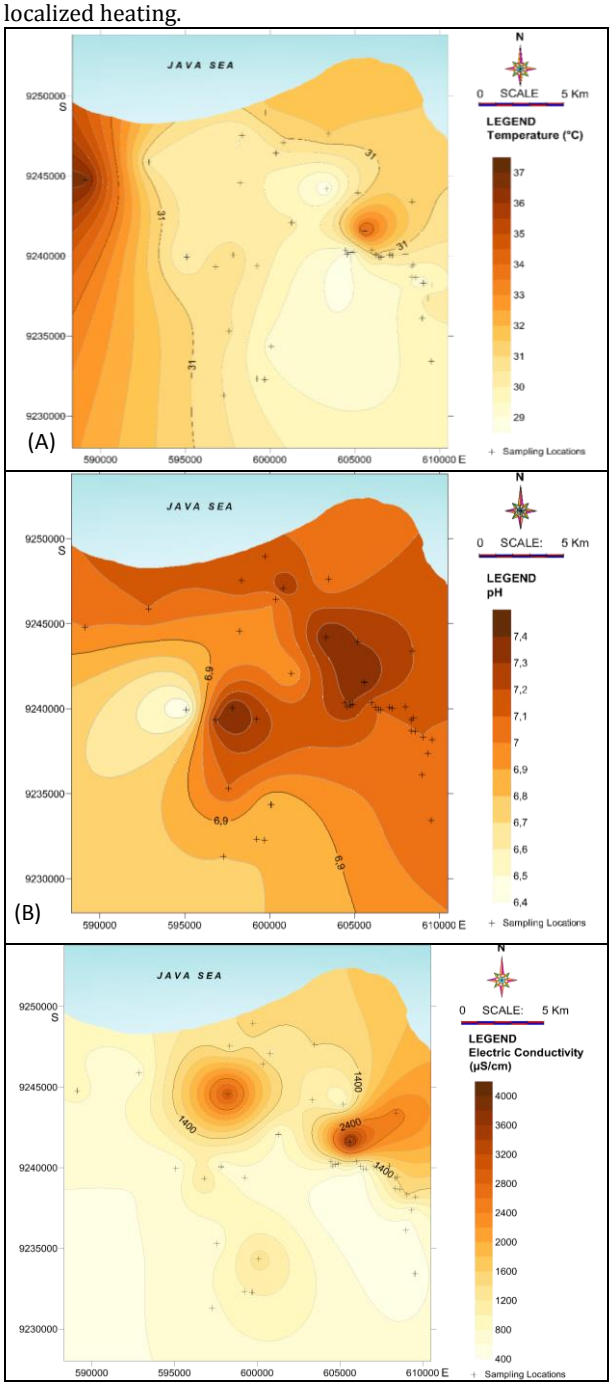

Fig. 3. A) Temperature spatial distribution. B) pH spatial distribution. C) EC spatial distribution

The in-situ pH values range from slightly acidic to slightly basic (6.4 to 7.4), with an average of 7.09 (Figure 3b). Despite the dominant carbonate lithology in the study area, pH values show no strong inclination towards either acidity or alkalinity, suggesting a relatively neutral groundwater system.

Electrical conductivity (EC) values show considerable variation, ranging from 468 to 4088 µS/cm, with an average of 1327 µS/cm (Figure 3c). Elevated EC values, especially those approaching the higher end of the range, suggest significant saline influence, which is likely due to seawater intrusion. In the eastern part of the study area, the presence of an extensive alluvial system, coupled with several rivers, provides pathways for seawater to migrate inland.

In the western part of the study area, groundwater is extracted using high-capacity pumps situated near the coastline. This anthropogenic activity could be exacerbating seawater intrusion into the aquifer. Furthermore, geological mapping suggests the presence of a fault system running from the western to the central part of Western Tuban, which may act as a conduit for seawater intrusion (Fig. 2). The fault potentially disrupts the groundwater system, allowing saline water to mix with the local groundwater. Elevated sulfate (SO_4^{2-}) concentrations north of the fault line further support the hypothesis of seawater intrusion being facilitated by fault-related pathways. However, direct evidence of the fault's influence on seawater intrusion, such as hydrogeophysical data or fault permeability studies, remains a subject for further investigation.

Table 1. Statistical information on physicochemical properties of the groundwater samples.

Parameter	Min	Max	Mean
pH	6.4	7.4	7.09
EC (µS/cm)	550	3950	1236.8
TDS (mg/L)	270	1960	614
T (°C)	28.6	36.7	30.71
Hardness (mg/L $CaCO_3$)	231.9	1658.3	439.87
Ca^{2+} (mg/L)	50.1	215.3	109.69
Mg^{2+} (mg/L)	0	25.5	1.19
Fe^{3+} (mg/L)	0	0.37	0.09
Mn^{2+} (mg/L)	0	0.2	0.03
K^{+} (mg/L)	1	181.2	27.24
Na^{+} (mg/L)	4	507.4	77.56
Li^{+} (mg/L)	0	0.4	0.02
NH_4^{+} (mg/L)	0	1	0.09
HCO_3^{-} (mg/L)	131.2	676.7	415.17
Cl^{-} (mg/L)	11.2	963	121.18
$SO_4^{=}$ (mg/L)	0	1455	116.88
NO_3^{-} (mg/L)	0	115.3	24.14

5.2 Major cations and anions geochemistry

5.2.1. Cation Concentrations

The average concentrations of major cations in the groundwater of Western Tuban, Indonesia, are ranked from highest to lowest as follows: Ca^{2+}, Na^{+}, K^{+}, Mg^{2+}, Fe^{3+}, NH_4^{+}, Mn^{2+}, and Li^{+}. The concentration of calcium (Ca^{2+}) averages 109.688 mg/L, with a range between 50.1 and 215.3 mg/L (Figure 4a). The elevated levels of Ca^{2+} indicate that the groundwater is classified as hard water; therefore, treatment may be necessary to reduce calcium content for certain uses.

Sodium (Na^{+}) concentrations vary significantly from 4 to 507.4 mg/L, with an average of 77.564 mg/L (Figure 4b). The potassium (K^{+}) concentrations range from 1 to 181.2 mg/L, with a mean value of 27.24 mg/L (Figure 4c). The high concentrations of sodium and potassium, particularly

in areas close to the coast, suggest potential seawater intrusion affecting groundwater quality, especially in regions where groundwater is extensively extracted for irrigation.

Magnesium (Mg^{2+}) concentrations are relatively low, averaging only 1.18 mg/L and ranging from 0 to 25.5 mg/L (Figure 4d). Despite the influence of carbonate rock formations in the region, the low magnesium levels may indicate a scarcity of dolomitic carbonate rocks in Western Tuban.

5.2.2. Anion Concentrations

The predominant anions in the groundwater are ordered as follows: HCO_3^-, Cl^-, SO_4^{2-}, and NO_3^- based on their average concentrations. Bicarbonate (HCO_3^-) values range from 131.2 to 676.7 mg/L with an average concentration of 415.17 mg/L (Figure 5a). The high bicarbonate levels are expected due to the carbonate lithology prevalent in Western Tuban, which contributes bicarbonate ions through mineral leaching processes.

Chloride (Cl^-) has a mean concentration of 121.18 mg/L and varies from 11.2 to 963 mg/L (Figure 5b). Higher chloride concentrations are predominantly found in the northern part of Western Tuban near the shoreline. Notably, one sample exhibited an anomalously high Cl^- value likely linked to over-extraction from agricultural wells situated close to the sea.

Sulfate (SO_4^{2-}) concentrations range from 0 to 1455 mg/L with an average of 116.87 mg/L (Figure 5c). The observed sulfate anomalies may stem from both natural processes and anthropogenic activities; potential natural sources include gypsum or anhydrite deposits within the karstic underground cave systems. Conversely, anthropogenic factors such as excessive fertilizer application near groundwater sources could also contribute to elevated sulfate levels.

Nitrate (NO_3^-) concentrations average 24.14 mg/L, with values ranging from 0 to 115.3 mg/L (Figure 5d). Elevated nitrate levels can arise from both natural processes—such as organic matter decomposition in soil—and anthropogenic influences including agricultural runoff or wastewater discharge from septic systems located near groundwater sources.

5.3 Hydrogeochemistry

The hydrogeochemical characteristics of the groundwater were assessed using geochemical facies analysis represented by Piper diagrams. These diagrams consist of two triangular plots for cations and anions and a diamond-shaped diagram that integrates both sets of data into a single point representing hydrochemical facies. This approach effectively illustrates the hydrochemical relationships among various groundwater samples.

The Piper trilinear diagram indicates that the groundwater primarily falls into calcium-sodium-potassium types for cations and predominantly bicarbonate types for anions (Figure 6). The observed shift from calcium-dominated cation water towards sodium and potassium types suggests ion exchange processes where calcium is replaced by sodium at exchange sites within clays or other minerals along the flow path. Additionally, this shift may indicate increased weathering of silicate minerals.

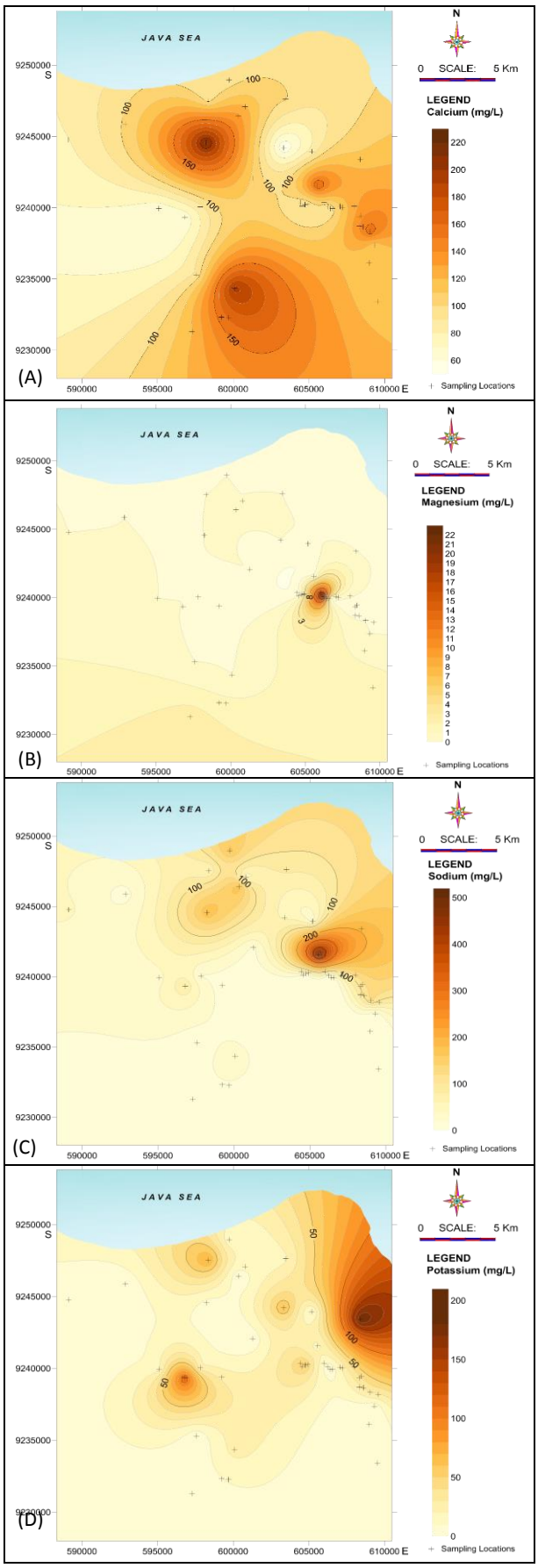

Fig. 4. A) Spatial distribution of Ca^{2+}. B) Spatial distribution of Mg^{2+}. C) Spatial distribution of Na^{+}. D) Spatial distribution of K^{+}

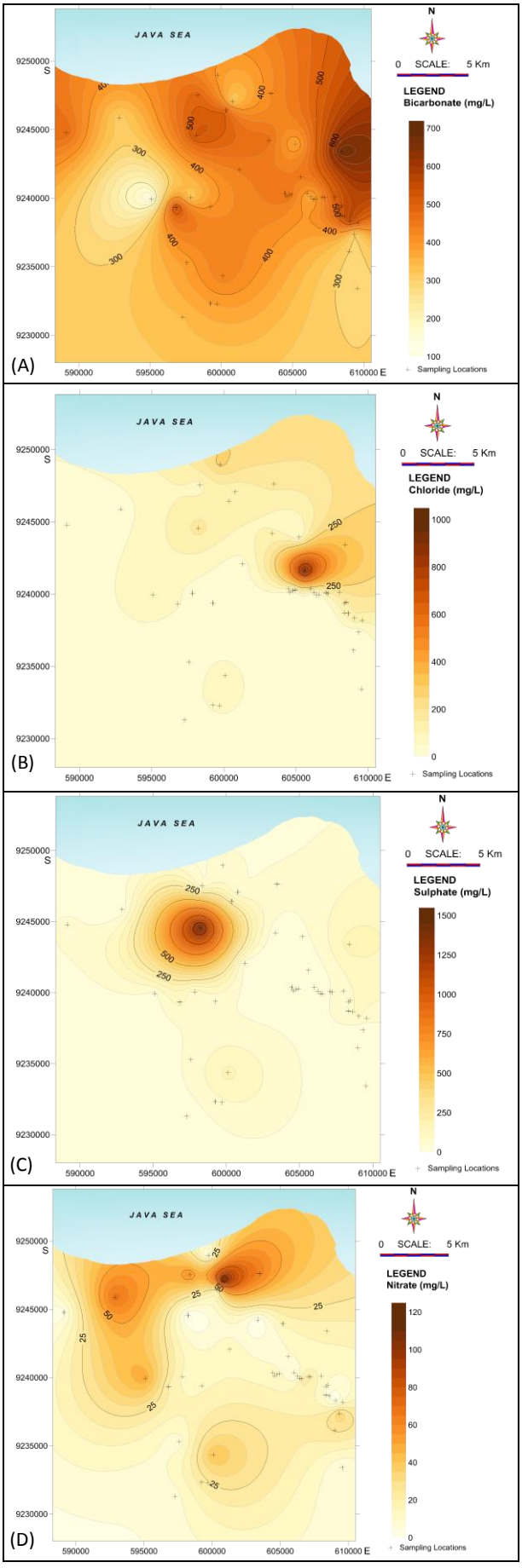

Fig. 5. A) Spatial distribution of HCO_3^-. B) Spatial distribution of Cl^-. C) Spatial distribution of SO_4^{2-}. D) Spatial distribution of NO_3^-.

The predominance of bicarbonate ions is consistent with the region's carbonate lithology; interactions between groundwater and these rocks release bicarbonate into solution. The transition from calcium-bicarbonate water types to sodium-chloride types may indicate either seawater intrusion—where saline water infiltrates coastal aquifers—or anthropogenic influences such as wastewater discharge.

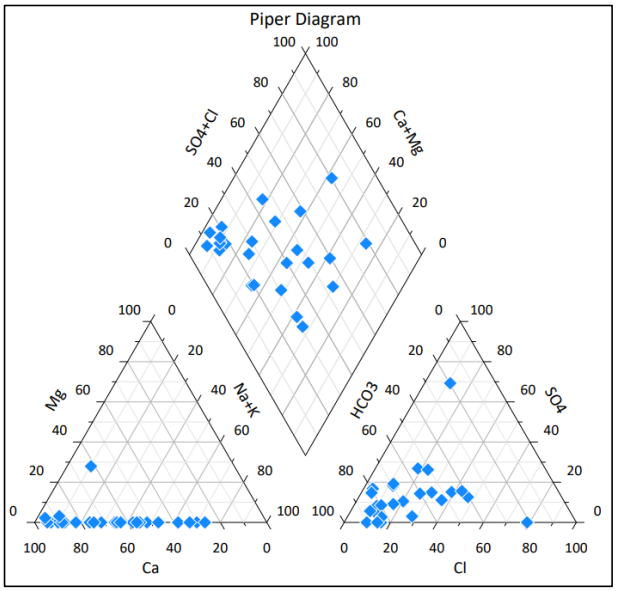

Fig. 6. Piper trilinear diagram (after Piper, 1944) depicting hydrogeochemical groundwater facies from the study area.

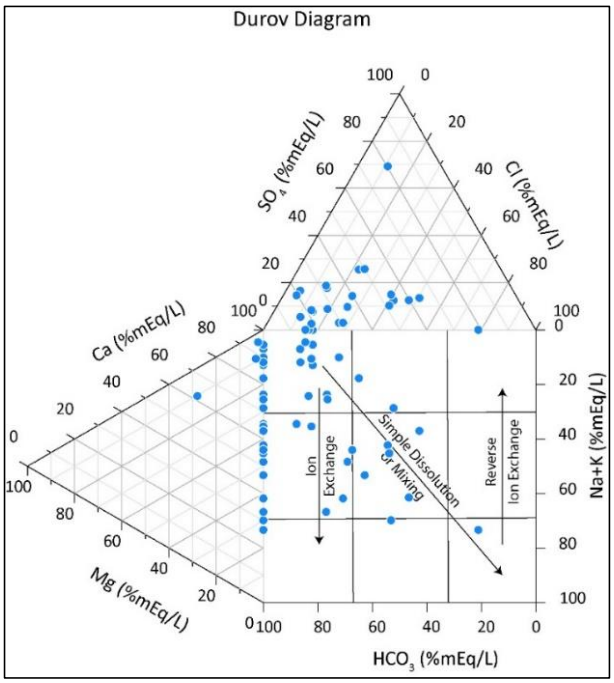

Fig. 7. Durov diagram (after Durov, 1948) depicting hydrogeochemical processes in groundwater as it moves through the aquifer.

To further delineate hydrochemical characteristics, a Durov diagram was constructed (Durov, 1948). The data plotted on this diagram reveal shifts towards ion exchange processes and simple dissolution or mixing phenomena (Figure 7). Groundwater interactions with clay minerals facilitate ion exchange where some calcium ions are substituted by sodium and potassium ions. This transition

reflects mixing with seawater intrusion that elevates sodium, potassium, and chloride concentrations while reducing relative bicarbonate levels.

Comparative analysis with similar carbonate settings in southern Java (Pambudi et al., 2022) shows that the groundwater in this study area exhibits more advanced contamination—both naturally occurring and anthropogenic—compared to findings from southern Java where water quality remains relatively pristine.

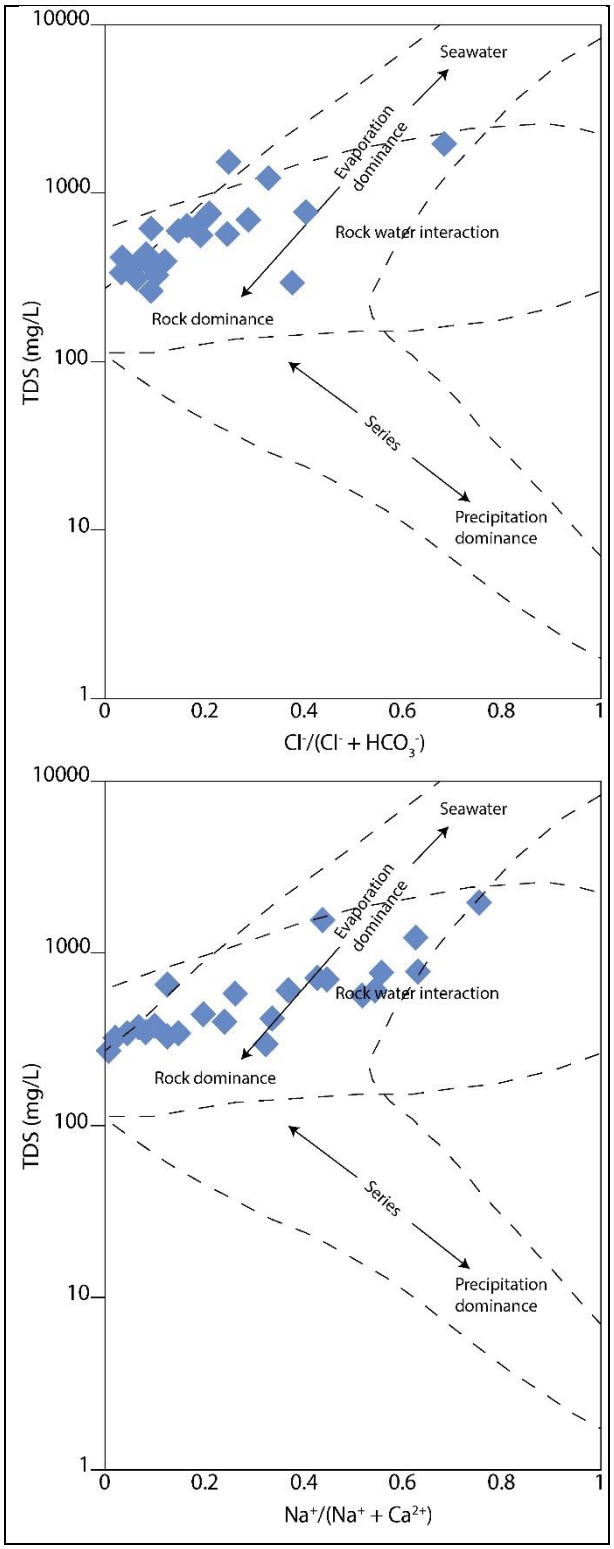

Fig. 8. Gibbs diagrams for hydrological controlling mechanism (after Gibbs, 1970).

Gibbs diagrams were employed to assess correlations between aquifer lithological characteristics and water composition across three fields: precipitation dominance, rock-water interaction dominance, and evaporation dominance. The majority of samples plotted within the rock-water interaction zone (Figure 8), indicating that rock weathering is a primary factor influencing groundwater hydrochemistry. While Gibbs diagrams provide insights into natural processes driving groundwater evolution, they do not adequately capture the complexities introduced by human activities affecting groundwater chemistry. This revision aims to enhance clarity and coherence while also addressing specific points raised by reviewers regarding detail and explanation within your manuscript.

5.4 Groundwater quality assessment

Several approaches are used to assess the quality of groundwater used for irrigation and drinking, such as the Wilcox and United States Salinity Laboratory (USSL) diagrams. Typically, both natural weathering processes and anthropogenic activities can influence the quality of drinking water.

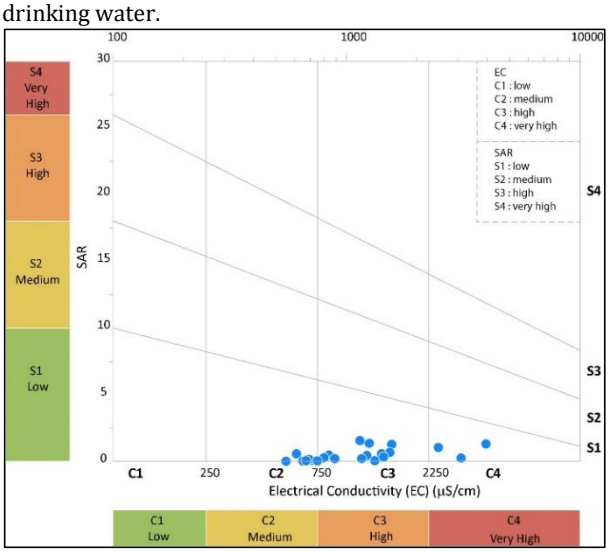

Fig. 9. Water quality ratings for agriculture (after Richards, 1954) based on electrical conductivity and sodium alkali rating (SAR).

The categorization of water used for irrigation is established by plotting the electrical conductivity (EC) and Sodium Absorption Ratio (SAR) values on the USSL diagram (Richards, 1954; Fig. 9). The TDS (total dissolved solids) in the groundwater's salinity directly impacts plant growth and impacts soil permeability, structure, and aeration. The Na+ concentration in water is an essential factor in determining water quality as it can affect the soil's characteristics and reduce its permeability. Irrigation with high sodium-depositing water is generally unsuitable as it can cause increased sodium deposition, which can negatively affect the soil. As a result, the use of SAR as a measure of the sodium (alkali) hazard in irrigation is considered more dependable as it is a crucial factor in determining the suitability of water for irrigation since it is directly connected to the adsorption of sodium by soil. An excessive amount of Na+ in comparison to Ca2+ and Mg2+ can result in reduced soil permeability, which ultimately hinders the water supply necessary for crops. The Sodium Adsorption Ratio (SAR) quantifies the ratio of sodium ions to calcium and magnesium ions in a water sample and is employed to predict the sodium hazard of high-carbonate waters, particularly when there is no residual alkali. SAR is

also employed to assess an overabundance of sodium or a scarcity of Ca2+ and Mg2+ content in water (Kalra and Maynard, 1991). The SAR is calculated with this formula:

$$SAR = \frac{Na^+}{\sqrt{(Ca^{2+}+Mg^{2+})/2}} \quad (1)$$

where the concentrations of all cations are expressed in milliequivalents per liter.

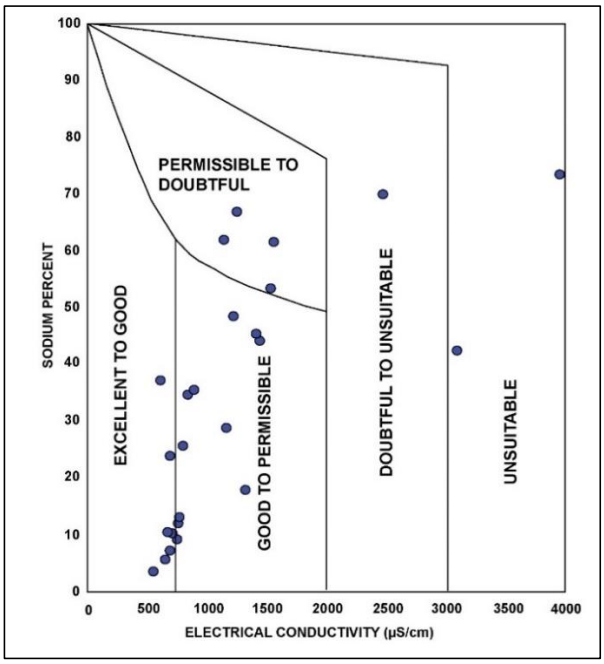

Fig. 10. Wilcox diagram (after Wilcox, 1995) showing electrical conductivity and the relationship between sodium percentage for the assessment of agricultural water quality.

The USSL diagram identifies four types of sodium hazards (S1, S2, S3, S4) and four types of salinity hazards (C1, C2, C3, C4). The level of salinity hazard can be an indicator of whether or not the water is suitable for irrigation (Ravikumar et al., 2011). Groundwater sources with low salt content (C1) can be used to water most plants and soils, with some leaching required. This can be done with normal watering methods, except for soils having low permeability. Water with medium salt content (C2) can be used if more salt is leached. Water with high salt content and low sodium (C3 and C4) can only be used for plants that can tolerate salt well and may not work well for soils that have restricted drainage. Even with good drainage, extra care is needed to manage salt levels, and only plants that can handle salt well should be chosen to be planted. Areas with high salinity water require particular attention regarding irrigation management. Based on the 25 samples (Figure 9), no samples belong to C1 and any S2, S3, or S4 category; eight samples (32%) are of C2S1 type indicating medium salinity-low sodium type, 14 samples fall into C3S1 implying high salinity-low sodium type (56%), and the rest (12%) are of C4S1 category suggesting very high-salinity low sodium type.

Wilcox (1995) developed a classification system for groundwater used in irrigation based on the correlation between the percentage of sodium (i.e., the concentration of sodium present in the irrigation water) and electrical conductivity. Percent sodium can be calculated using the following equation:

$$\%Na = \frac{(Na^+ + K^+)\times 100}{(Ca^{2+}+Mg^{2+}+Na^+ + K^+)} \quad (2)$$

where the concentrations of Ca2+, Mg2+, Na+, and K+ are represented in meq/L. In cases when the sodium concentration is high in irrigation water, it is more probable that sodium ions are more likely to be adsorbed by clay particles, pushing out calcium and magnesium ions. The exchange of sodium ions from the water for calcium and magnesium ions in the soil lowers permeability, which can gradually lead to soil with inadequate internal drainage. Based on the 25 samples (Figure 10), 7 (28%) belong to excellent to good; 11 (44%) good to permissible; 4 (16%) permissible to doubtful; 1 (4%) doubtful to unsuitable; 2 (8%) unsuitable.

6. Conclusion

Groundwater is a vital resource for various applications, including those in karstic regions. Our objective was to examine the formation and development of a typical karst groundwater system, as well as the impact of human activities. We collected water samples, characterized their hydrogeochemical properties, and analyzed the relationships using spatial, statistical, and graphical methods. The statistical analysis revealed that the cation abundance in the study area's groundwater follows the order of $Ca^{2+}>Na^{+}>K^{+}>Mg^{2+}$, while the anion abundance is $HCO_3^{-}>Cl^{-}>SO_4^{2-}>NO_3^{-}$. The majority of water samples are fresh, with TDS values below 1000 mg/L, and only a few exceptions. HCO_3^{-} is the dominant anion in fresh water. The groundwater in the study area is primarily of the HCO_3–Ca+Mg type, with some Na+K–SO_4+Cl. The area is influenced by silicate mineral weathering, carbonate lithology dissolution, seawater intrusion, and other human activities. The groundwater evolves through ion exchange with clay minerals and mixing with seawater. The hydrological mechanism that controls groundwater chemistry is mainly the interaction of rock and water. From the groundwater quality assessment, all groundwater samples have medium to high salinity that requires attention prior to usage for irrigation. Most of the samples which fall on high salinity levels (C3 and C4 types) need space with open drainage, and only crops exhibiting high levels of salt tolerance should be selected for cultivation. Based on the level of sodium and other cations, only 12% of all the samples are categorized as doubtful and unsuitable for soil drainage.

Acknowledgements

The authors would like to express their gratitude to the Laboratory of Geophysics of Mining Engineering ITB for their opportunity to conduct this hydrogeological study in Tuban Regency.

References

Adimalla, N., Li, P., Venkatayogi, S., 2018. Hydrogeochemical Evaluation of Groundwater Quality for Drinking and Irrigation Purposes and Integrated Interpretation with Water Quality Index Studies. Environ. Process. 5, 363–383. https://doi.org/10.1007/s40710-018-0297-4

Aditia, D.N., 2013. Geologi dan lingkungan pengendapan Formasi Tuban Daerah Kerek dan sekitarnya

Kabupaten Tuban Provinsi Jawa Timur. Universitas Pembangunan Nasional Veteran Yogyakarta, Yogyakarta.
Antonellini, M., Nannoni, A., Vigna, B., De Waele, J., 2019. Structural control on karst water circulation and speleogenesis in a lithological contact zone: The Bossea cave system (Western Alps, Italy). Geomorphology 345, 106832. https://doi.org/10.1016/j.geomorph.2019.07.019
Asikin, S., 1992. Peta Geologi Lembar Banyumas.
Badan Pusat Statistik Kabupaten Tuban, 2023. Jumlah Curah Hujan di Kabupaten Tuban (mm), 2020-2022.
BAKOSURTANAL, 1999. Peta rupabumi digital Indonesia 1:25000 Sheet 1509-224 Jenu.
Blake, J.M., Walton-Day, K., Gallegos, T.J., Yager, D.B., Teeple, A., Humberson, D., Stengel, V., Becher, K., 2022. New Geochemical Framework and Geographic Information System Methodologies to Assess Element Occurrence, Persistence, and Mobility in Groundwater and Surface Water. Minerals 12, 411. https://doi.org/10.3390/min12040411
Durov, S.A., 1948. Natural waters and graphic representation of their composition. Dokl Akad Nauk SSSR 59, 87–90.
Elango, L., Kannan, R., 2007. Chapter 11 Rock–water interaction and its control on chemical composition of groundwater, in: Developments in Environmental Science. Elsevier, pp. 229–243. https://doi.org/10.1016/S1474-8177(07)05011-5
Fitchen, J., 1988. Anthropology and Environmental Problems in the U.S.: The Case of Groundwater Contamination. Practicing Anthropology 10, 5–20. https://doi.org/10.17730/praa.10.3-4.v387p7463005862q
Ford, D., Williams, P.W., 2010. Karst hydrogeology and geomorphology, [Rev. ed.]. ed. John Wiley & Sons, Chichester, England.
Foster, S.S.D., 2001. The interdependence of groundwater and urbanisation in rapidly developing cities. Urban Water 3, 185–192. https://doi.org/10.1016/S1462-0758(01)00043-7
Gibbs, R.J., 1970. Mechanisms Controlling World Water Chemistry. Science 170, 1088–1090. https://doi.org/10.1126/science.170.3962.1088
Glynn, P.D., Plummer, L.N., 2005. Geochemistry and the understanding of ground-water systems. Hydrogeol J 13, 263–287. https://doi.org/10.1007/s10040-004-0429-y
Kalra, Y.P., Maynard, D.G., 1991. Methods manual for forest soil and plant analysis (No. Information Report NOR-X-319E). Northwest Region, Northern Forestry Centre, Forestry Canada, Edmonton, Alberta.
Kaufmann, G., Romanov, D., 2019. The initial phase of cave formation: Aquifer-scale three-dimensional models with strong exchange flow. Journal of Hydrology 572, 528–542. https://doi.org/10.1016/j.jhydrol.2019.03.053
Nijhawan, A., Howard, G., 2022. Associations between climate variables and water quality in low- and middle-income countries: A scoping review. Water Research 210, 117996. https://doi.org/10.1016/j.watres.2021.117996
Pambudi, S., Sulistijo, B., Yudiantoro, D.F., Haty, I.P., 2022. Studi hidrogeokimia air tanah di daerah Kebumen bagian barat, Indonesia. Jurnal Ilmiah Geologi Pangea 61–67. https://doi.org/10.31315/jigp.v9i1sp.9411.g5226
Parise, M., Gabrovsek, F., Kaufmann, G., Ravbar, N., 2018. Recent advances in karst research: from theory to fieldwork and applications. SP 466, 1–24. https://doi.org/10.1144/SP466.26
Piper, A.M., 1944. A graphic procedure in the geochemical interpretation of water-analyses. Trans. AGU 25, 914. https://doi.org/10.1029/TR025i006p00914
Ravikumar, P., Somashekar, R.K., Angami, M., 2011. Hydrochemistry and evaluation of groundwater suitability for irrigation and drinking purposes in the Markandeya River basin, Belgaum District, Karnataka State, India. Environ Monit Assess 173, 459–487. https://doi.org/10.1007/s10661-010-1399-2
Richards, L.A., 1954. Diagnosis and Improvement of Saline Alkali Soils, Agriculture. US Department of Agriculture, Washington DC.
Sarrazin, F., Hartmann, A., Pianosi, F., Wagener, T., 2018. V2Karst V1.0: A parsimonious large-scale integrated vegetation-rechargemodel to simulate the impact of climate and land coverchange in karst regions (preprint). Hydrology. https://doi.org/10.5194/gmd-2017-315
Stevanović, Z., 2015. Characterization of Karst Aquifer, in: Stevanović, Z. (Ed.), Karst Aquifers—Characterization and Engineering, Professional Practice in Earth Sciences. Springer International Publishing, Cham, pp. 47–125. https://doi.org/10.1007/978-3-319-12850-4_3
Sullivan, P.L., Macpherson, G.L., Martin, J.B., Price, R.M., 2019. Evolution of carbonate and karst critical zones. Chemical Geology 527, 119223. https://doi.org/10.1016/j.chemgeo.2019.06.023
van Bemmelen, R.W.W., 1949. The Geology of Indonesia. Government Printing Office, Nijhoff, The Hague.
Wilcox, L.V., 1995. Classification and use of irrigation waters. US Department Agricultural 19.